

**NOVEL MULTIFUNCTIONAL PLATINUM
NANODENDRITES AS THERANOSTIC AGENTS
IN CANCER IMAGING AND RADIOTHERAPY
TREATMENT**

MUHAMMAD AFIQ BIN KHAIRIL ANUAR

UNIVERSITI SAINS MALAYSIA

2021

**NOVEL MULTIFUNCTIONAL PLATINUM
NANODENDRITES AS THERANOSTIC AGENTS
IN CANCER IMAGING AND RADIOTHERAPY
TREATMENT**

by

MUHAMMAD AFIQ BIN KHAIRIL ANUAR

**Thesis submitted in fulfilment of the requirements
for the degree of
Doctor of Philosophy**

October 2021

ACKNOWLEDGEMENT

In the name of Allah, The Most Gracious, and The Most Merciful

Without any shred of doubt, my gratefulness is toward my Creator; The Creator of this world and everything within. He is The All-Knowing, whom without His grace, I would not be able to grasp even a tiny drop of His knowledge.

My most profound appreciation extends toward my supervisor, Dr Wan Nordiana Wan Abd Rahman, for her relentless guidance that started even before this PhD began. Also, toward my co-supervisor, Professor Dr Khairunisak Abdul Razak, whom I rarely met, yet without her input and supports, this journey would be much more difficult.

Not to forget, thanks to all the staff of USM and Hospital USM that helped me during the works' completion (Mdm. Norhayati, Mr Reduan, Mr Zaky and colleagues), as well as my research team (Jo, Belle, Emi, Nashrul, Amirah and Mr Safri), whom I shared my bittersweet experiences all these years. And of course, this work will not be realized without the financial support by the Malaysian Ministry of Higher Education through the FRGS grant (No:203/PPSK/6171160) and the MyBrain (MyPhD) scholarship.

Finally, special gratitude toward my stepfather, Mohd Azli Mat, who supported me and my family since I was 12, and thus, I dedicated this PhD thesis for you, Papa. Of course, for my beloved Mama, Julita Yusof, nothing in this world is large enough to contain my love and gratefulness toward you. Also, my dear wife, Ardhawiah, I lost count on how much sacrifice she shouldered in having a full-time-studying husband like me. Truly, thank you. Thank you.

TABLE OF CONTENTS

ACKNOWLEDGEMENT	ii
TABLE OF CONTENTS	iii
LIST OF TABLES	ix
LIST OF FIGURES	xi
LIST OF ACRONYMS, ABBREVIATIONS AND SYMBOLS	xvii
ABSTRAK	xxii
ABSTRACT	xxiv
CHAPTER 1 INTRODUCTION	1
1.1 Cancer Prevalence, Diagnosis, and Treatment	1
1.2 Radiobiological Impact of Ionizing Radiation	5
1.3 The Importance of Contrast Agents and Radiosensitizers in Cancer Management	8
1.3.1 Nanomaterials as Potential Theranostic Agent.....	14
1.4 Problem Statement.....	17
1.5 Objective of Study	19
1.6 Scope of Study	19
1.7 Thesis Outline.....	20
CHAPTER 2 LITERATURE REVIEW	22
2.1 The Fabrication and Characterization of Platinum Nanoparticles.....	22
2.1.1 Multiple Pathways of Nano-platinum Production.....	22
2.1.2 Nanoparticle Characterization Methods for Biological Applications.....	26
2.2 Theranostic Applications of Nanoparticles	30

2.2.1	Radiotherapy for Cancer Treatment	30
2.2.2	Theranostics in Cancer Management	32
2.2.3	The Application of High-Z Nanoparticles as Theranostic Agents.	33
2.3	The Mechanisms of Radiosensitization Effect by High-Z Nanoparticles	43
2.3.1	Physical Mechanisms	44
2.3.2	Chemical Mechanisms.....	52
2.3.3	Biological Mechanisms	56
CHAPTER 3 METHODOLOGY		61
3.1	Platinum Nanodendrite Synthesis Method	63
3.2	Characterization of PtNDs.....	64
3.2.1	Transmission Electron Microscopy (TEM).....	64
3.2.2	Dynamic Light Scattering (DLS)	64
3.2.3	Atomic Absorption Spectrometry (AAS).....	65
3.2.4	X-ray Diffraction Spectroscopy (XRD)	66
3.2.5	PtNDs' pH Measurement	67
3.3	Biocompatibility Assessments of PtNDs.....	67
3.3.1	Cell Culture Maintenance and Protocols.....	67
3.3.2	PtNDs' Cytotoxicity Evaluation.....	69
3.3.3	Assessment of PtNDs Localization in Cells.....	71
3.4	The Evaluation of PtNDs as Contrast Agent in Diagnostic Radiology	73
3.4.1	Sample Preparation for Diagnostic Imaging	73
3.4.2	Computed Tomography Imaging	74
3.4.3	Planar X-ray Imaging	76

3.4.4	Fluoroscopy Imaging.....	78
3.5	PtNDs' Radiosensitization Effects in Radiotherapy.....	80
3.5.1	Sample Preparations for Radiotherapy Procedures	80
3.5.2	Radiotherapy Irradiation Procedures	82
3.5.2(a)	6 MV Photon Beam Therapy	82
3.5.2(b)	6 MeV Electron Beam Therapy	83
3.5.2(c)	150 MeV Proton Beam Therapy	84
3.5.3	Validation of Radiotherapy Dose	85
3.5.4	Clonogenic Assay Analysis.....	89
3.5.5	Quantification of the PtNDs' Radiosensitization Effect	92
3.5.6	Quantification of ROS Generation	96
3.6	Statistical Analysis.....	97
 CHAPTER 4 RESULTS		98
4.1	Synthesis and Characterization of the PtNDs.....	98
4.1.1	PtND Fabrication Process.....	98
4.1.2	PtND Characterization Process	99
4.1.2(a)	Pt Concentration Within the PtNDs Suspension.....	100
4.1.2(b)	Assessment of PtND Size Using TEM and Zetasizer	101
4.1.2(c)	X-Ray Diffraction Spectrometry.....	103
4.1.2(d)	PtNDs' pH Measurement.....	104
4.2	PtNDs' Biocompatibility Assessment	105
4.2.1	PtNDs' Cytotoxicity Evaluation.....	105
4.2.2	The Evaluation of PtNDs' Cellular Uptake and Localization	111

4.3	Assessment of PtND Performance as a Diagnostic Contrast Agent.....	115
4.3.1	Computed Tomography Imaging	115
4.3.2	Planar X-ray Imaging	118
4.3.3	Fluoroscopy Imaging.....	121
4.4	PtNDs' Radiosensitization Effects	123
4.4.1	Validation of Radiotherapy Dose	124
4.4.2	PtNDs' Radiosensitization Effect in Radiotherapy	126
	4.4.2(a) 6 MV Photon Beam Irradiation.....	126
	4.4.2(b) 6 MeV Electron Beam Irradiation.....	132
	4.4.2(c) 150 MeV Proton Beam Irradiation	138
4.4.3	Correlation of PtNDs' Radiosensitization Effect with ROS Production.....	145
4.5	Result Summary.....	150
CHAPTER 5 DISCUSSION.....		151
5.1	The Synthesis and Characterization of Platinum Nanodendrites	151
5.1.1	The Effect of Reaction Temperature on the PtND Synthesis.....	160
5.2	The Biocompatibility of PtNDs	163
5.2.1	The Cytotoxicity of the PtNDs	164
5.2.2	The Internalization of PtNDs by Cells	170
5.3	PtNDs as an X-ray Contrast Agent.....	172
5.3.1	PtNDs Attenuated X-Ray Better than Iodinated Contrast Agent	174
5.3.2	PtND Sizes Proportionally Influence the X-Ray Attenuation Property	175
5.4	PtNDs as a Radiosensitizer in Radiotherapy	181

5.4.1	Quantification of Radiosensitization Effect by PtNDs.....	181
5.4.1(a)	The Cell Colony Quantification Method	181
5.4.1(b)	Cell Survival Model Fitting	182
5.4.2	Radiosensitization by PtNDs in Different Radiotherapy Beams.....	185
5.4.2(a)	Photon Beam Radiotherapy	186
5.4.2(b)	Electron Beam Therapy	195
5.4.2(c)	Proton Beam Therapy	200
5.4.3	The Role of ROS in the PtNDs' Radiosensitization Effect	204
5.4.3(a)	PtNDs Affected the ROS Level in Cells Without Irradiation.....	205
5.4.3(b)	The Effect of PtND-radiotherapy Combination toward Intracellular ROS Level	209
CHAPTER 6 CONCLUSION		216
6.1	The Synthesis and Characterization of PtNDs.....	216
6.2	The Biocompatibility of PtNDs	216
6.3	The Potential of PtNDs as an X-ray Contrast Agent	217
6.4	The Radiosensitization Effect of PtNDs in Radiotherapy	217
6.5	The Potential of PtNDs as Theranostic Agent.....	217
6.6	Future Direction and Recommendations	218
REFERENCES.....		219
APPENDICES		
Appendix A: Mass Attenuation Coefficient Chart		
Appendix B: Calculations		
Appendix C: Powder Diffraction File™ (PDF®)		

Appendix D: The Microscopic Image of MCF-7 And MDA-MB-231 Cells

Appendix E: Planar X-ray Imaging Data

Appendix F: Turnitin Screening Report

LIST OF PUBLICATIONS AND PRESENTATIONS

LIST OF TABLES

		Page
Table 1.1	Examples of side effects associated with radiotherapy treatment with respect to the treatment site (Mohan <i>et al.</i> , 2019).....	10
Table 1.2	The distribution of radiotherapy centres and equipment based on the country developing index (IAEA, 2021).....	12
Table 3.1	The parameters of PtND fabrication process.....	63
Table 3.2	The components of the solution within the sample tubes.....	81
Table 4.1	The Pt yield concentration measured using AAS.....	100
Table 4.2	The parameters for concentrating the PtND suspensions.....	101
Table 4.3	Comparison of fabricated PtND particle size, hydrodynamic size, zeta potential and polydispersity index with respect to the amount of K ₂ PtCl ₄ used.....	103
Table 4.4	The dose corrections for photon and electron beam therapy in the radiosensitization study.	124
Table 4.5	The survival curve of control samples irradiated with 6 MV photon beams and their corresponding parameters.	127
Table 4.6	The survival curve of 29 nm PtND-treated samples irradiated with 6 MV photon beam and its corresponding parameters.....	128
Table 4.7	The survival curve of 36 nm PtND-treated samples irradiated with 6 MV photon beam and its corresponding parameters.....	129
Table 4.8	The survival curve of 42 nm PtND-treated samples irradiated with 6 MV photon beam and its corresponding parameters.....	130
Table 4.9	The survival curve of 52 nm PtND-treated samples irradiated with 6 MV photon beam and its corresponding parameters.....	131
Table 4.10	The survival curve of control samples irradiated with 6 MV electron beam and its corresponding parameters.....	133
Table 4.11	The survival curve of 29 nm PtND-treated samples irradiated with 6 MeV electron beam and its corresponding parameters.	134
Table 4.12	The survival curve of 36 nm PtND-treated samples irradiated with 6 MeV electron beam and its corresponding parameters.	135

Table 4.13	The survival curve of 42 nm PtND-treated samples irradiated with 6 MeV electron beam and its corresponding parameters.	136
Table 4.14	The survival curve of 52 nm PtND-treated samples irradiated with 6 MeV electron beam and its corresponding parameters.	137
Table 4.15	The survival curve of control samples irradiated with 150 MeV proton beam and its corresponding parameters.	139
Table 4.16	The survival curve of 29 nm PtND-treated samples irradiated with 150 MeV proton beam and its corresponding parameters.	140
Table 4.17	The survival curve of 36 nm PtND-treated samples irradiated with 150 MeV proton beam and its corresponding parameters.	141
Table 4.18	The survival curve of 42 nm PtND-treated samples irradiated with 150 MeV proton beam and its corresponding parameters.	142
Table 4.19	The survival curve of 52 nm PtND-treated samples irradiated with 150 MeV proton beam and its corresponding parameters.	143
Table 4.20	The comparison of SER_{MID} of the PtNDs with respect to the PtND sizes and type of radiotherapy.	144
Table 4.21	The comparison of SER_{50} of the PtNDs with respect to the PtND sizes and type of radiotherapy.	144
Table 5.1	Comparison of DMR under different reference conditions.	184
Table 5.2	Examples of the studies that assessed the radiosensitization effect of high-Z nanoparticles in 6 MV photon beam therapy.	187
Table 5.3	Examples of studies that have performed the DCF assay measurement to assess the change in ROS level in PtNP-treated cells.	208
Table 5.4	The change in ROS level in samples after 3 Gy and 6 Gy photon beam radiotherapy (PhT), compared to the respective SER_{MID}	211
Table 5.5	The change in ROS level in samples after 3 Gy and 6 Gy electron beam therapy (EBT), compared to their respective SER_{MID}	211
Table 5.6	The change in ROS level in samples after 3 Gy and 6 Gy proton beam therapy (PrT), compared to the respective SER_{MID}	211
Table 5.7	The comparison of SER_{50} and ROS generation, %, by a different type of nanoparticles.	213

LIST OF FIGURES

		Page
Figure 1.1	The estimated number of new cancer cases globally (top chart) and in Malaysia (bottom chart) by 2020 (IARC, 2020).	2
Figure 1.2	Comparison of depth dose curves for a 10 MV photon beam and a 10 MeV proton beam (shown with and without an SOBP). This figure shows a lower entrance dose and absence of exit dose for the proton beam compared to the photon beam (Image adapted from Ladra and Yock (2014), Figure 1, Page 114).	5
Figure 1.3	Direct and indirect action of DNA damages due to radiation.	8
Figure 1.4	Overall survival of HNC treated with SBRT regimens with different treatment modalities (Image adapted from Park <i>et al.</i> (2021)).	11
Figure 1.5	The raised concern on the need for advanced contrast agents and radiosensitizers for current cancer radiotherapy.....	14
Figure 2.1	Categories of platinum nanoparticle synthesis methods.	23
Figure 2.2	Relative percentage depth dose (PDD) of three different types of radiotherapy.	32
Figure 2.3	(A) The cell survival of 4T1 cells treated with radiotherapy alone (control) and radiotherapy + HfO ₂ NPs treatment with respect to radiotherapy dose. (B) The change in tumour volume in mice treated with radiotherapy and HfO ₂ NPs. (C) The HU intensities of HfO ₂ NPs compared to the iodinated contrast agent in CT imaging (The images were extracted from Li <i>et al.</i> (2020), Figure 2, Figure 4, and Figure 5, Page 4-6).....	40
Figure 2.4	(A) The illustration of SeAuFe-EpC physical structure and (B) the high-resolution TEM image of SeAuFe-EpC NPs. (Images adapted from Liu <i>et al.</i> (2020a), Scheme 1 and Figure 1, Page 4-5).....	41
Figure 2.5	The cross-section (probability) of three major types of photon-matter interactions with respect to the atomic number of the absorber material, Z, and the photon energy, MeV (Power, 2021a).....	45
Figure 2.6	The graphs of photoelectric effect mass attenuation coefficient of platinum and soft tissue for photon energy between 1 keV to 15 MeV. Theoretical data was obtained from the National Institute of Standards and Technology (Berger and Hubbell, 1987).....	46

Figure 2.7	The three stages of water radiolysis upon ionizing radiation exposure, and the resulting species including ROS that can induce oxidative stress to biological medium (Image adapted from Le Caër (2011), Scheme 1, Page 239).	54
Figure 2.8	The mechanism of cellular apoptosis led by the radiation-induced ROS (Image adapted from Howard <i>et al.</i> (2020), Figure 1, Page 4).....	57
Figure 2.9	The complex mechanisms behind the radiosensitization effect of high-Z nanoparticles.....	60
Figure 3.1	The flow chart of the research methodology.....	62
Figure 3.2	An example of a 96-well plate containing cell samples with different amounts of cell viability. Prestobblue® remained blue in the wells without cells. The red Prestobblue® signifies the presence of viable cell populations in the wells.	70
Figure 3.3	The flow of the cellular PtND uptake analysis using the ‘Analyze Particle’ macro in ImageJ software. The original image (top left) was thresholded, resulting in red marks over the PtNDs. The yellow ROI was drawn on the thresholded image (top right). Then, Analyze Particle was performed, giving the results as shown in the bottom images.	72
Figure 3.4	The Visipaque™ 320 stock solution.	73
Figure 3.5	(A) An example of the PtND sample contained in a 3 mL syringe and (B) the CT imaging setup.	74
Figure 3.6	An example of a CT image slice with ROIs drawn on the cross-sectional images of the syringes.	75
Figure 3.7	Sample placements inside a 96-well plate for planar X-ray imaging.....	77
Figure 3.8	Planar X-ray imaging setup.....	77
Figure 3.9	An example of the samples’ grey value measurement by using the ImageJ software.....	78
Figure 3.10	(A) Samples of PtNDs (labelled as C, D, E, and F), ICA (labelled as B), and distilled water (labelled as A) contained inside 1.5 mL microcentrifuge tubes. (B) Fluoroscopy imaging was performed in an erect position, with the samples sandwiched in between the solid water phantoms.....	79

Figure 3.11	An example of the pixel value quantification process in the fluoroscopy image. The contrast solution was located at the cylindrical part of the tube, and the pixel values were recorded along the middle to ensure the uniformity of the attenuation thickness.	80
Figure 3.12	The schematic diagram (A) and photograph image (B) of the set-up for MV photon beam irradiation.....	83
Figure 3.13	The schematic diagram (A) and the photographed image (B) of the set-up for MV electron beam irradiation.	84
Figure 3.14	The schematic diagram (A) and the photographed image (B) of the set-up for proton beam irradiation.	85
Figure 3.15	Comparison of the setup for control (A) and the setup for sample irradiations (B) (PhT and EBT irradiations).....	86
Figure 3.16	The schematic of the film placement in proton beam therapy irradiation for dose validation purpose.....	87
Figure 3.17	(A) The placement of sample tubes on top of film versus film only (control). (B) Example of irradiation setup (PhT), with 1.5 cm bolus placed on top of the samples and films.....	87
Figure 3.18	An example of image of digitized films for photon beam therapy irradiation.	88
Figure 3.19	Example of calibration curve, which equates the absorbed dose in control condition to the respective measured net optical density. The absorbed dose was the average of the measured dose from 5 ROIs drawn on each film strip.....	89
Figure 3.20	An example of the scanned 6-well plates for the clonogenic assay procedure. The yellow arrow marks the centre of the scanner, as well as the scan direction. The caps of the plates were scanned altogether for plate identification.	90
Figure 3.21	The example of an extracted well image (A) and its thresholded image (B). The blue colour in the thresholded image represents 100 % intensity. The colour gradually changes to yellow as the intensity dropped. The white area is the deleted background that contains no cells.	91
Figure 3.22	An example of Linear Quadratic (LQ) curves fitted based on the survival fraction (SF) of the control samples (solid line) and PtNDs samples (dashed line). Blue and red arrows represent the data extrapolations for SER_{50} and DMF quantification, respectively. The Mean Inactivation Dose (MID) is the area under	

	the curve, which can be obtained by integrating the curve from 0 Gy to 10 Gy.	93
Figure 4.1	(A) Example of unsuccessful (left-hand tube) and successful (right-hand tube) PtND synthesis product. (B) A row of successfully fabricated PtNDs from Sample #1 until #4 (left to right). Visually, no difference in the opacity of the solutions can be observed, although they were fabricated with different amount of precursor concentration.	99
Figure 4.2	The TEM images of PtNDs fabricated from (A) 5.19 mg K_2PtCl_4 , (B) 10.38 mg K_2PtCl_4 , (C) 15.57 mg K_2PtCl_4 and (D) 20.76 mg K_2PtCl_4 , respectively.	102
Figure 4.3	The XRD patterns of (a) 29 nm PtNDs, (b) 36 nm PtNDs, (c) 42 nm PtNDs, and (d) 52 nm PtNDs.	104
Figure 4.4	The average pH level of PtNDs, DMEM, and PtND-mixed DMEM.	105
Figure 4.5	The cytotoxic effect of PtNDs of different sizes on the HeLa cell line.	107
Figure 4.6	The effect of PtND length of exposure on 52 nm PtNDs cytotoxicity toward HeLa cell line.	107
Figure 4.7	The cytotoxicity effect of 52 nm PtNDs on HeLa, MCF-7 and MDA-MB-231 cell lines.	108
Figure 4.8	Cell viability of HeLa, MCF-7 and MDA-MB-231 cells after exposure with PtNDs' supernatant at the corresponding PtND concentration.	110
Figure 4.9	Example of fixed control (A) and PtND-treated (B) HeLa cells stained with crystal violet dye under 100× magnification. Red, yellow, and black arrows marked the cell nuclei, cytoplasm, and PtND particles.	111
Figure 4.10	The microscopic images of HeLa cells treated with 29, 36, 42 and 52 nm PtNDs under 100× magnification. An image of untreated HeLa cells (Control) was added as a comparison.	112
Figure 4.11	Number of particles taken up by HeLa cells with respect to the prescribed PtND sizes.	113
Figure 4.12	Mean particle diameter of PtNDs taken up by HeLa cells with respect to the prescribed PtND sizes.	114

Figure 4.13	The measured mean HU of distilled water, 1 mM iodinated contrast agent and PtNDs of different sizes.	116
Figure 4.14	The mean CNR of 1 mM iodinated contrast agent and PtNDs of different sizes.....	117
Figure 4.15	The mean gray values (MGV) of the tested materials irradiated with 81 kVp planar X-ray.....	119
Figure 4.16	The mean gray value (MGV) of the tested materials with respect to the X-ray tube potential, kVp.	120
Figure 4.17	The fluoroscopic image of stock iodinated contrast agent contained with a microcentrifuge tube. The red and yellow numbers marked in the image are the pixel values. Note that the pixel values of iodine (red) are much lower than the surrounding air (yellow).	122
Figure 4.18	Mean pixel value (MPV) of different materials within a fluoroscopic image. Lower MPV signifies better X-ray attenuation property.....	122
Figure 4.19	The dose verification data for (A) photon, (B) electron, and (C) proton beam therapy. The green zone marked the tolerance level of the data (5 % deviation from unity). The data that deviates beyond the tolerance level was marked with *.....	125
Figure 4.20	The ROS generation in HeLa cells after the photon beam radiotherapy (PhT) irradiation. Statistically significant differences between the controls and the PtND groups are indicated by * $p < 0.001$, ** $p < 0.05$ and <i>ns</i> for not significantly different. The bar for the non-irradiated control samples is labelled as <i>c</i> , which is taken as 100 % of the relative intensity.....	147
Figure 4.21	The ROS generation in HeLa cells after the electron beam therapy (EBT) irradiation. Statistically significant differences between the controls and the PtND groups are indicated by * $p < 0.001$, ** $p < 0.01$ and *** $p < 0.05$. The bar for the non-irradiated control samples is labelled as <i>c</i> , which is taken as 100 % of the relative intensity.	148
Figure 4.22	The ROS generation in HCT 116 cells after the proton beam therapy (PrT) irradiation. Statistically significant differences between the controls and the PtND groups are indicated by * $p < 0.001$, ** $p < 0.01$, *** $p < 0.05$ and <i>ns</i> for not significantly different. The bar for the non-irradiated control samples is labelled as <i>c</i> , which is taken as 100 % of the relative intensity.....	149
Figure 4.23	The summary of results in this thesis.	150

Figure 5.1	The summary of the possible X-ray attenuation effect by nanoparticles of different sizes.....	180
Figure 5.2	An image of a scanned six-well plate containing densely packed cell colonies.	182
Figure 5.3	LQ curves of PtND treated and control cells after 6 MV photon irradiation.	184
Figure 5.4	The comparison of SER_{MID} of the PtNDs with respect to the PtND sizes and type of radiotherapy.	186
Figure 5.5	The illustration of primary radiation-nanoparticle interactions and the escape of secondary radiations from the nanoparticle's surface with respect to the nanoparticle size. The circle with solid and dotted lines represents the small and big nanoparticles, respectively. Primary radiations are portrayed as black arrows, and their interactions with the nanoparticle produced secondary radiations (grey arrows).....	193
Figure 5.6	A brief illustration of nanoparticle-radiation interaction.....	195

LIST OF ACRONYMS, ABBREVIATIONS AND SYMBOLS

%	Percentage
μ	Micro
μ/ρ	Mass attenuation coefficient
^{192}Ir	Iridium-192
3D-CRT	Three-dimensional conformal radiation therapy
AAS	Atomic absorption spectrometry
ANOVA	Analysis of Variance
AP	Anterior-posterior
AuNP	Gold nanoparticles
BED	Biologically effective dose
BiNP	Bismuth nanoparticles
BiNR	Bismuth nanorod
BiONP	Bismuth oxide nanoparticles
CERT	Contrast-enhanced radiotherapy
cGy	Centigray
cm	Centimetre
CM	Complete growth medium
cm ²	Square centimetre
CNR	Contrast-to-noise ratio
CO ₂	Carbon dioxide
CT	Computed tomography
DCF	2',7'-dichlorofluorescein
DEF	Dose enhancement factor
DHR-123	Dihydrorhodamine-123
DICOM	Digital Imaging and Communications in Medicine
DLS	Dynamic light scattering
d_{max}	Depth of maximum dose
DMEM	Dulbecco's Modified Eagles Medium
DMF	Dose modification factor
DMSO	Dimethyl sulfoxide
DNA	Deoxyribonucleic acid

DSB	Double strand break
EBT	Electron beam therapy
EDTA	Ethylenedinitrilotetraacetic acid
EDX	Energy-dispersive X-ray spectroscopy
EF	Enhancement factor
ELS	Electrophoretic light scattering
EpCAM	Epithelial cell adhesion molecules
EPR	Enhanced permeability and retention
FBS	Fetal bovine serum
FDA	Food and Drug Association
Fe ₃ O ₄	Iron oxide
FTIR	Fourier transform infrared spectroscopy
G ₂	Second checkpoint of growth phase (cell cycle)
Glu-GNP	Glucose-capped gold nanoparticles
GNP	Gold nanoparticles
GSH	Glutathione
GTV	Gross tumour volume
Gy	Gray (radiation dose unit)
H	Hydrogen
H ₂ DCF-DA	2',7'- dichlorodihydro-fluorescein diacetate
H ₂ O ₂	Hydrogen Peroxide
HCl	Hydrochloric acid
Hf	Hafnium
Hf:Hap	Hafnium-doped hydroxyapatite
HfO ₂	Hafnium oxide
HNC	Head and neck cancer
HU	Hounsfield unit
IAEA	International Atomic Energy Agency
ICA	Iodinated contrast agent
ICDD	International Center for Diffraction Data
ICP-MS	Inductively coupled plasma mass spectrometry
IGRT	Image-guided radiotherapy
IMRT	Intensity-modulated radiotherapy

INFORMM	Institute for Research in Molecular Medicine
K ₂ PtCl ₄	Potassium tetrachloroplatinate (II)
kV	Kilovoltage
kVp	Peak kilovoltage
LEE	Low-energy electrons
LET	Linear energy transfer
LINAC	Linear accelerator
LQ	Linear Quadratic
M	Mitotic phase (cell cycle)
MAGICA	Methacrylic Ascorbic in Gelatin Initiated by Copper with Agarose added
MeV	Mega-electron volt
mg/L	milligram per litre
MGV	Mean gray value
MID	Mean inactivation dose
mL	Millilitre
mM	Millimolar
mmol/L	Milli mol per litre
MPV	Mean pixel value
MRI	Magnetic resonance imaging
mtDNA	Mitochondrial DNA
MTT	3-[4,5-dimethylthiazol-2-yl]-2,5-diphenyl tetrazonium bromide
MV	Megavoltage
MVCT	megavoltage computed tomotherapy
NAC	N-acetylcysteine
nm	Nanometre
NP	Nanoparticle
OAR	Organ at risk
PA	Photoacoustic
PBS	Phosphate buffered saline
PCNA	Proliferating cell nuclear antigen
Pd	Palladium

PDF®	Powder Diffraction File™
PDI	Polydispersity index
PE	Photoelectric effect
PEG	Polyethylene glycol
PhT	Photon beam radiotherapy
PP	Pair production
PrT	Proton beam therapy
Pt	Platinum
PTCOG	Particle Therapy Co-Operative Group
PtND	Platinum Nanodendrite
PtNP	Platinum nanoparticles
PtO	Platinum oxide
PTV	Planning target volume
RBE	Relative biological effectiveness
Redox	Oxidation-reduction
ROI	Region of interest
ROS	Reactive oxygen species
rpm	Revolution per minute
RT	Radiotherapy
S	Synthesis phase (cell cycle)
SBRT	Stereotactic body radiation treatment
SeNP	Selenium nanoparticles
SER ₅₀	Sensitization enhancement ratio based on 50 % SF
SER _{MID}	Sensitization enhancement ratio based on MID
SF	Survival fraction
SOBP	Spread-out Bragg peak
SPCCT	Sophisticated spectral photon-counting computed tomography
SPION	Superparamagnetic iron oxide nanoparticles
SRS	Stereotactic radiosurgery
SSB	Single-strand break
SSD	Source-to-surface distance
TEM	Transmission electron microscopy

TMRE	Tetramethylrhodamine ethyl ester perchlorate
TPPMS	triphenylphosphine mono-sulfonate
USM	Universiti Sains Malaysia
UV	Ultraviolet
WHO	World Health Organization
XRD	X-ray diffraction spectroscopy
Z	Atomic number
Z/A	The ratio of an atomic number to nucleon number

***PLATINUM NANODENDRITE* PELBAGAI FUNGSI BAHARU SEBAGAI
EJEN TERANOSTIK UNTUK PENGIMEJAN KANSER DAN RAWATAN
RADIOTERAPI**

ABSTRAK

Nanopartikel dengan nombor atom yang tinggi telah dikaji secara pesat sebagai ejen radioteranostik kerana mempunyai kadar penyerapan X-ray yang tinggi dan farmakokinetik yang bagus. Namun, kajian ke atas ejen berasaskan platinum sangat terhad walaupun bahan ini telah digunakan secara meluas dalam bidang kimoterapi. Justeru, kajian ini dibuat bertujuan untuk menghasilkan bahan yang baru, iaitu *Platinum Nanodendrite* (PtND) sebagai ejen radioteranostik. PtND yang dihasilkan dalam kajian ini mempunyai permukaan bercaj negatif dan berbentuk dendrit. Empat saiz PtND telah disediakan untuk kajian teranostik. Semua PtND ini menunjukkan kadar toksik yang rendah terhadap model-model sel yang digunakan dalam kajian ini bagi kepekatan di bawah 0.1 mM. Sekiranya kepekatan dinaikkan melebihi had itu, kadar toksik PtND meningkat bergantung kepada saiz partikel, jenis sel dan tempoh inkubasi. Penyelidikan teranostik PtND terbahagi kepada dua bahagian, iaitu bahagian diagnostik dan radioterapi. Kemampuan diagnostik PtND diuji menggunakan kepekatan PtND maksimum, iaitu 1.0 mM untuk meningkatkan kontras dalam imej sinar-X. PtND dengan saiz yang berbeza telah dibandingkan dengan ejen kontras iodin menggunakan tiga jenis alat sinar-X (tomografi berkomputer, fluoroskopi, dan sinar-X menyatah). Hasil kajian menunjukkan kadar penyerapan sinar-X oleh PtND jauh lebih baik dari iodin dengan kepekatan yang sama. Kadar penyerapannya juga

bergantung kepada saiz PtND, yang mana PtND lebih besar menyerap sinar-X lebih baik berbanding PtND yang kecil. Kajian radioterapi pula dibuat menggunakan tiga jenis radiasi, iaitu sinar foton 6 MV (PhT), radiasi elektron 6 MeV (EBT), dan radiasi proton 150 MeV (PrT). Sebelum diradiasi, sel HeLa telah dirawat menggunakan PtND berkepekatan 0.1 mM. Kemudian, sel tersebut didedahkan dengan dos radiasi yang berbeza-beza. Penilaian klonogenik sel itu menunjukkan yang PtND berjaya meningkatkan kepekaan sel tersebut terhadap radiasi. Peningkatan tersebut juga bergantung kepada saiz PtND dan jenis radiasi yang digunakan. Kadar pemekaan tertinggi direkodkan oleh gabungan PtND bersaiz 29 nm dengan PhT (SER=2.54). Manakala untuk PrT dan EBT, PtND bersaiz 36 nm (SER=1.38) dan 42 nm (SER=1.83) adalah lebih baik. Seterusnya, penilaian DCF tidak menunjukkan sebarang perkaitan antara gabungan rawatan radiasi dan PtND terhadap perubahan tahap spesis oksigen radikal (ROS) di dalam sel. Ini menunjukkan bahawa tekanan oksidatif berkemungkinan bukan punca utama di sebalik kesan pemekasaran PtND. Kesimpulannya, kajian ini telah berjaya menghasilkan ejen radioteranostik yang baru, iaitu PtND. Ejen ini adalah lebih baik berbanding iodine untuk pengimejan sinar-X, dan mampu memeka sel terhadap radioterapi. Justeru, PtND berpotensi untuk meningkatkan keberkesanan pengesanan dan rawatan kanser berasaskan radiasi mengion.

**NOVEL MULTIFUNCTIONAL PLATINUM NANODENDRITES AS
THERANOSTIC AGENTS IN CANCER IMAGING AND RADIOTHERAPY
TREATMENT**

ABSTRACT

High-Z nanoparticles have been studied over the years as a potential radio-theranostic agent due to their high X-ray absorption and good pharmacokinetic properties. However, only a few platinum-based agents have been reported in the literature, despite its wide usage in chemotherapy (i.e., cisplatin). Thus, this work aims to study platinum nanoparticles, Platinum Nanodendrites (PtND), as a novel theranostic agent. The PtNDs fabricated in this work possessed a dendritic shape with a negatively charged surface. Four PtND sizes were prepared for theranostic evaluations (29 nm, 36 nm, 42 nm, and 52 nm). *In-vitro* biocompatibility assessment revealed that the PtNDs of all sizes were non-cytotoxic for the particle concentration of up to 0.1 mM. Furthermore, the PtNDs' toxicity also depended on PtNDs' size, cell type, and incubation period. The theranostic evaluation of PtNDs was separated into diagnostic and radiotherapy sections. The diagnostic evaluation was performed with the maximum available PtND concentration, 1.0 mM, to maximize their image contrast in X-ray images. The PtNDs of different sizes were compared with the commercial iodinated contrast agent in three X-ray modalities (CT, fluoroscopy, and planar X-ray). The result in all imaging systems evidenced better attenuation of PtNDs over iodinated contrast agent at equivalent concentration. The contrast enhancement is also size-dependent, where larger PtNDs exhibited higher X-ray attenuation than the smaller

ones. The radiotherapy evaluation involved a study on the radiosensitization effects of PtNDs in three different types of radiotherapy: 6 MV photon radiotherapy, 6 MeV electron beam therapy, and 150 MeV proton beam therapy. HeLa cells were treated with 0.1 mM of PtNDs of different sizes and subjected to increasing radiation doses. The clonogenic assay evaluations revealed that the PtNDs successfully enhanced the radiosensitivity of HeLa cells, depending on the particle size and types of radiotherapy. The maximum radiosensitization effect was observed in the combination of 29 nm PtNDs with PhT (SER=2.54). 36 nm and 42 nm PtNDs produced the highest radiosensitization in PrT (SER=1.38) and EBT (SER=1.83), respectively. DCF assay assessment shows that the ROS induced by the PtND-radiation combinations may not be the major determining factors that catalyse the PtNDs' radiosensitization effect. In conclusion, this work has successfully developed and characterized the theranostic potential of PtNDs. This study provides a platform for theranostic multimodal approaches in diagnostic imaging and radiotherapy to improve cancer treatment efficacy and outcomes.

CHAPTER 1

INTRODUCTION

1.1 Cancer Prevalence, Diagnosis, and Treatment

Cancer is the uncontrollable spread of abnormal cells, which can affect almost any part of the body. 18.1 million new cancer cases were reported globally in 2018, and it rises to 19.3 million by 2020 (Bray *et al.*, 2018; IARC, 2021; Sung *et al.*, 2021). According to WHO, cancer has caused the death of more than 9.9 million global populations, making it the second leading cause of death worldwide in recent years (WHO, 2021). Figure 1.1 shows the estimated number of new cancer cases by 2020. Breast, lung, and colorectum cancer were the most significant contributor to new cancer cases in 2020, accounting for 11.7 %, 11.4 %, and 10 % of the total new cases globally. Whereas in Malaysia, the fraction of breast and colorectal cancer cases were much greater, accounting for 17.3 % and 13.6 % of the national total new cancer cases, respectively. It was projected that there would be around 28.4 million new cancer cases worldwide in 2040, a whopping 47 % increase of new cases compared to 2020 (Sung *et al.*, 2021).

WHO has categorized the cause of cancer into physical, chemical, biological carcinogens (WHO, 2021). This includes the risk factors such as external and environmental carcinogens (e.g., asbestos, arsenic, etc.), alcohol and tobacco consumption, dietary patterns, viral infections, and inactive lifestyles (Wu *et al.*, 2016; Connor, 2017; Grosso *et al.*, 2017; WHO, 2021). Primarily, cancer prevalence is associated with the socio-economic developments, ageing, and growth of populations (Bray *et al.*, 2018; Sung *et al.*, 2021).

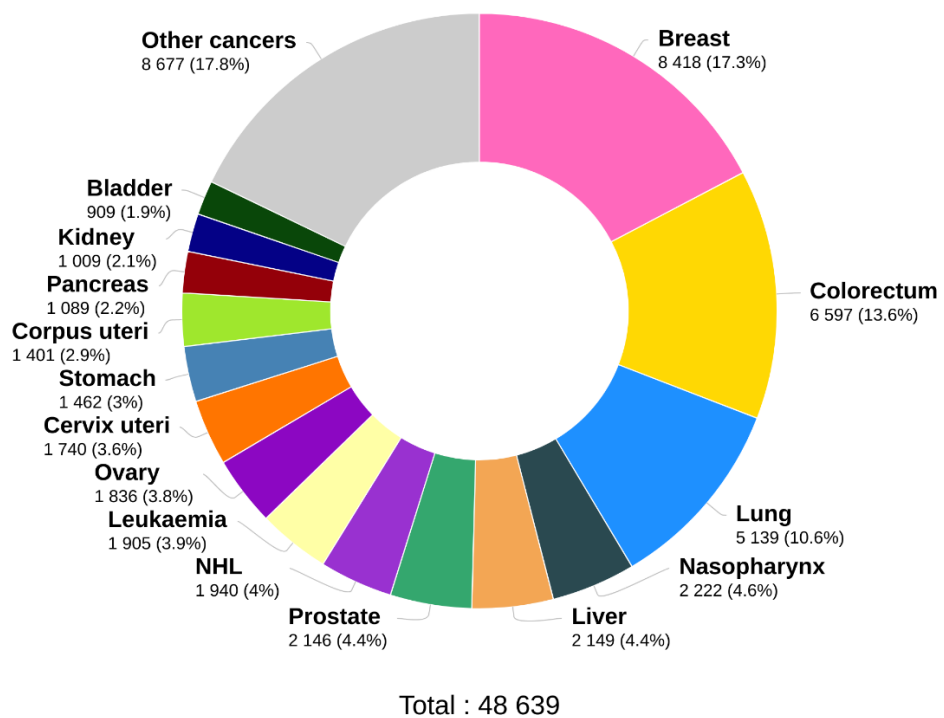
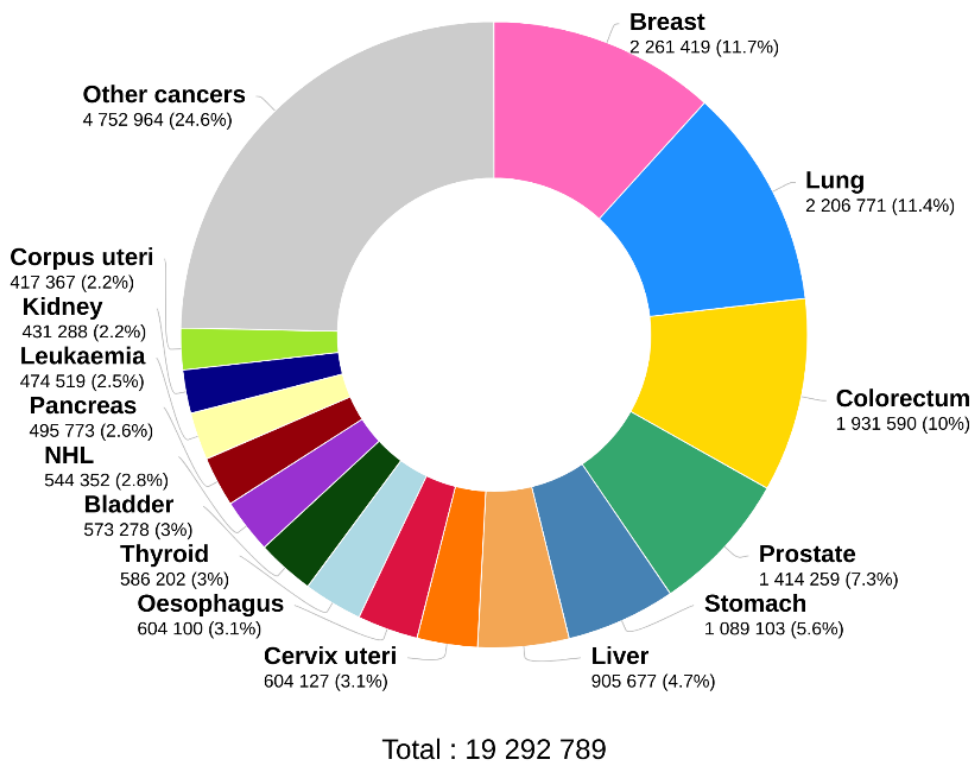


Figure 1.1 The estimated number of new cancer cases globally (top chart) and in Malaysia (bottom chart) by 2020 (IARC, 2020).

New cancer therapy options are flourishing in recent years to address the growing cancer burden, such as targeted therapy (Sawyers, 2019; van de Stadt *et al.*, 2021), immunotherapy (Riveiro-Barciela *et al.*, 2020), and hormonal therapy (Abraham and Staffurth, 2020; Del Río *et al.*, 2020). However, conventional options such as chemotherapy, radiotherapy, and surgery remain as the primary route of cancer management (Kwatra *et al.*, 2013). A hefty 60 % of cancers cases require radiotherapy within the treatment regime (Mohan *et al.*, 2019). These conventional treatments were also touched by the advance in technology. For example, the previously non-specific chemotherapeutic agents now can be functionalized with carriers to deliver them precisely to cancer sites (Li *et al.*, 2019a; Yafout *et al.*, 2021). Conventional surgery can now be accompanied by robotic aid, which dramatically reduces the surgeons' workload (Baek *et al.*, 2021).

New and advanced technologies also being developed in radiotherapy; some have transitioned into clinical phases and becomes routine techniques, including stereotactic radiation therapy (stereotactic radiosurgery (SRS), stereotactic body radiation treatment (SBRT)) (Ricco *et al.*, 2017; Abel *et al.*, 2019), image-guided radiation therapy (IGRT) (Rosenberg *et al.*, 2019), and helical tomotherapy (Jeraj *et al.*, 2004; Lee *et al.*, 2021; Öztunali *et al.*, 2021). These new and advanced radiotherapy techniques boast over the conventional 3D conformal radiation therapy (3D-CRT) as possessing better dose conformity to the tumour, hence limiting the toxicity and side effects to the nearby organs at risk (OARs) (Lee *et al.*, 2021). This is proven by several clinical trial reports that show a significantly reduced rate of acute, subacute, and chronic toxicities while improving tumour control compared to

conventional radiotherapy (Joo *et al.*, 2017; Rosenberg *et al.*, 2019; Öztunali *et al.*, 2021).

Additionally, there is an increasing number of heavy particle beam centres worldwide (Grau *et al.*, 2020). The facilities use the high linear energy transfer (LET) particles such as neutrons, protons, helium, or carbon ions as dose delivery mediums. Despite being the most resource-demanding among all ionizing radiation therapy facilities, the superior treatment quality of particle-beam radiotherapy over X-rays are unquestionable due to the unique dose profile of the particle radiations, which is especially important in the management of cancers located nearby the radiosensitive OARs such as head and neck cancers (Jensen, 2020). This is due to heavy particle radiation's unique characteristic. The dose profile of the heavy particle beam and photon beam is shown in Figure 1.2. The figure clearly shows that the proton beam's entrance and exit radiation dose is vastly superior to the photon beam, making it the best candidate for better dose localization in the tumour.

The current advancement in tumour treatment, especially with the application of particles beam, will lead to more sophisticated and efficient treatment techniques. Effective treatment can be optimally achieved with technological advancement in beam delivery and by understanding and improving the radiobiological impact of ionizing radiation on cancer cells.

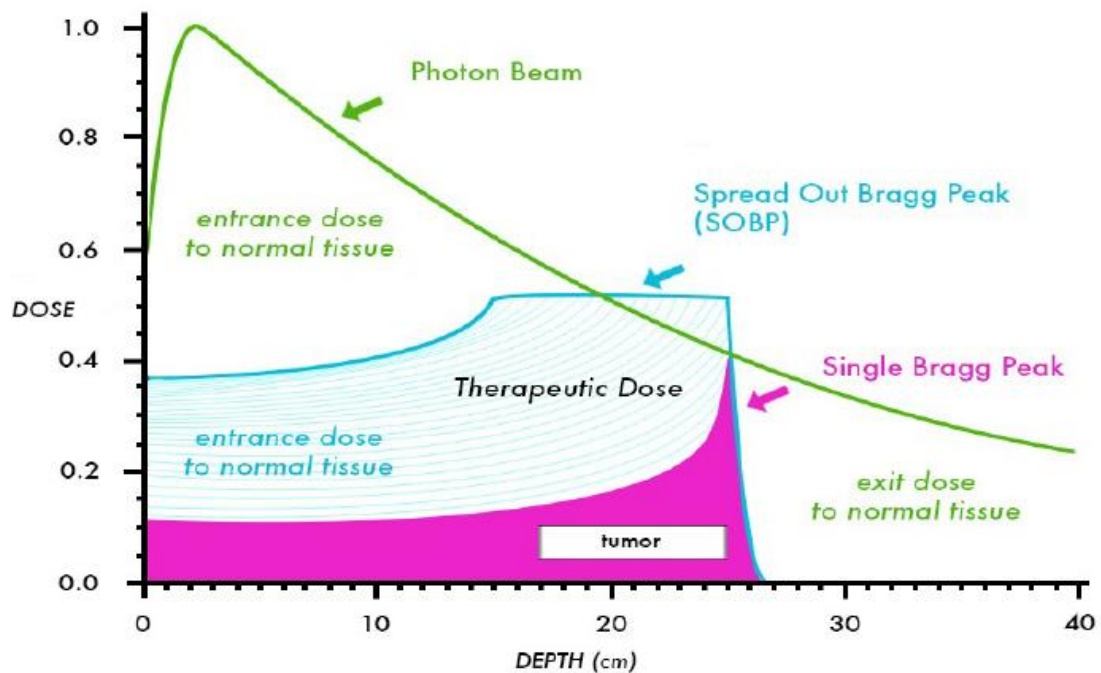


Figure 1.2 Comparison of depth dose curves for a 10 MV photon beam and a 10 MeV proton beam (shown with and without an SOBP). This figure shows a lower entrance dose and absence of exit dose for the proton beam compared to the photon beam (Image adapted from Ladra and Yock (2014), Figure 1, Page 114).

1.2 Radiobiological Impact of Ionizing Radiation

Radiotherapy implements ionizing radiations that deposit energy in their pathway and hence cause damage to the cells of the tissues. Clinical radiation beams come in various forms and sources, primarily photons (X-rays, gamma rays) and particles beam (electrons, protons, neutrons) that possess enough energy to excite electrons from their orbital within the atoms to form ions (Zeman *et al.*, 2020). In radiotherapy, a linear accelerator (LINAC) accelerates electrons to reach the kinetic energies of more than several megavoltages (MV) before bombarding them into a high-Z target to produce a spectrum of polyenergetic X-ray. This MV X-ray is highly energetic in that it can penetrate deep into the patients' body to reach the targeted

tumour, hence depositing their energy along the way and cause genetic changes resulting in cancer cell death.

The high energy X-ray beam is more practical for cancer radiotherapy than low kV X-rays because of higher beam penetration that can reach deep-seated tumours, produce lower skin dose, higher dose rate, flatter beam profile, and smaller penumbra (Stanton *et al.*, 2010). The LINAC also can be used as the electron beam source by simply removing the X-ray target from the accelerated electron path. The photon and electron beam undergoes different interaction with biological material and deposits their energy through different mechanisms.

The photoelectric effects, Compton scattering, and pair production are common interactions in clinical photon energy ranges (Cherry and Duxbury, 2019). The probability of each interaction (termed as the ‘interaction cross-section’) is different depending on the radiation quality and the interacting materials. In essence, photoelectric effects, Compton scattering, and pair production predominate at low, intermediate, and high X-ray energy, respectively (Power, 2021b).

Charged particles such as protons and electrons can create trails of ionizations and excitations along its path, dissipating its energy along the path until it subsequently comes into rest. A charged particle can dissipate its energy via two types of interactions: a) collision interaction and b) radiative interaction. While collision interactions involve the loss of energy via excitation and ionization of atoms, radiative interaction of charged particles differ in a way that the energy is lost via photon emission, usually by Bremsstrahlung (braking) radiation (Bushberg and Boone, 2011).

Following the radiation interaction, the ionization and excitation of atoms in the subjected medium will occur. As the molecules in the medium are atoms bonded

together, the ionization of one or more atoms in the molecules can cause the collapse of molecular structures (Zeman *et al.*, 2020). When ionizing radiations interact with biological media, biological molecules such as proteins and enzymes denature, causing damages to the cellular environment. This field of knowledge is termed radiobiology: a medical science field that delves into the biological effect of ionizing radiation on living tissues (Connor (2019)).

The most critical cellular structure is DNA, a group of genes that govern all the cellular functions, and hence become the most vulnerable target to radiation damage. Any damage to these macromolecules can lead to failure of cellular functions, which eventually will cause cell death. The damage that may occur can be estimated by assuming 1 Gy of radiation dose in a cell nucleus can produce roughly 2×10^5 ionizations, causing around 100 single-strand breaks and 40 double-strand breaks of DNA (Mayles *et al.*, 2007).

The mechanism of cell damage upon radiation exposures can be divided into direct and indirect actions (Connor, 2019). Direct action of cell damage occurs when ionizing radiation hit the atomic structures of DNA molecules directly, causing damage to molecules due to the ionization of the atoms. Indirect action happens when the ionizing radiation interacts with surrounding molecules (usually water), causing ionization and producing radicals such as hydroxyl OH, superoxide anion O^{2-} and others (Connor, 2019). These free radicals are highly reactive and capable of damaging DNA structures upon contact. Figure 1.3 illustrates the direct and indirect damage caused by ionizing radiations to a DNA strand. Although DNA damage is commonly correlated with cell death upon ionizing radiation exposure, there have been increasing evidence that other organelles such as endoplasmic reticulum, ribosome,

mitochondria, lysosome and cell membrane are also affected by radiation damage (Wang *et al.*, 2018).

Recently, many studies have investigated a new method in increasing optimal radiobiological impact to the cancer cells by applying radiosensitizer. The application of contrast agent and radiosensitizer seems to be a promising technique in enhancing DNA damage and cell death in tumours and elevating radiotherapy efficacy. These agents also can alleviate some of the limitations of the current-gen radiotherapy systems, which will be debriefed further in the following section.

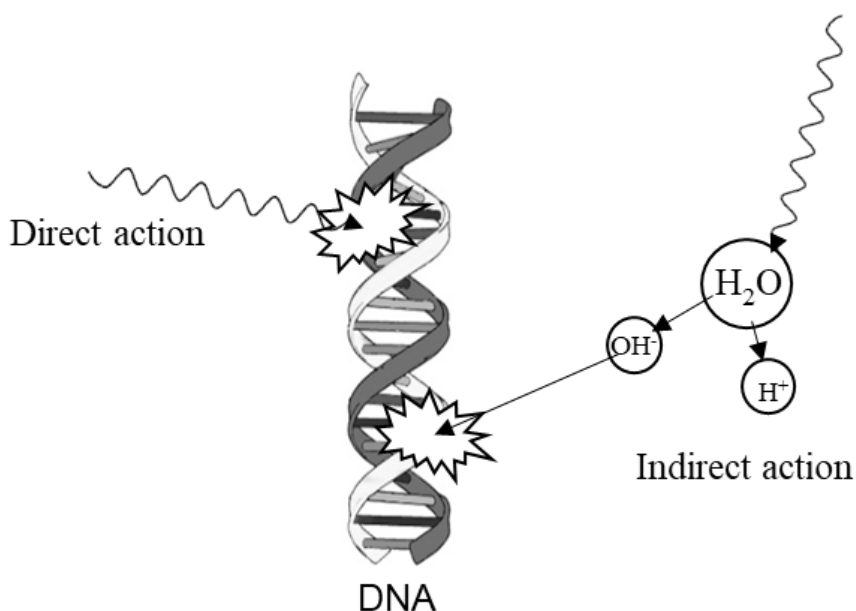


Figure 1.3 Direct and indirect action of DNA damages due to radiation.

1.3 The Importance of Contrast Agents and Radiosensitizers in Cancer Management

Since the discovery of X-rays and radioactivity more than 100 years ago, ionizing radiation has been used extensively worldwide for medical imaging and radiotherapy (Zeman *et al.*, 2020). The primary objective of cancer treatment using

ionizing radiation never really change since then: to deliver the maximum dose to the targeted tumour while minimizing the radiation hazard to the surrounding healthy tissues (Grégoire *et al.*, 2020; Kaanders *et al.*, 2020). The advancements in radiotherapy technologies, as mentioned in the previous section are all revolved around this objective.

Despite that, the side effect of radiotherapy never ceased to persist (Mohan *et al.*, 2019). The exact localization of dose to the tumour remains a considerable hurdle to be surpassed due to the nature of external radiation delivery: it needs to pass through healthy tissues to reach the commonly deep-seated tumours. The radiation also scatters upon interaction, compromising the neighbouring healthy tissues. Some cancer patients are more radiosensitive than others. Around 5 % of them received limited radiation dosage to avoid the adverse side effects (Mohan *et al.*, 2019).

Table 1.1 summarizes some examples of adverse side effects associated with radiotherapy treatments. Multiple post-treatment remedies were used to treat these side effects (Mohan *et al.*, 2019). However, this option will introduce additional costs at the expense of the patients' quality of life. Thus, it is essential to continue discovering ways to maximize the treatment efficacy and healthy tissue sparing in the current and upcoming radiotherapy treatment regimes.

The effectiveness of SBRT in enhancing the biological effective dose (BED) is unquestionable as multiple clinical reports already proved the superior outcome of cancer management by using stereotactic body radiation treatment (SBRT) over the conventional therapies (Joo *et al.*, 2017; Rosenberg *et al.*, 2019). This favourable outcome entices the oncologists to escalate the radiation dose further to improve the

tumoricidal effectiveness. However, this venture is also hindered by the constraint of the dose to the nearby organs at risk (Yadav *et al.*, 2021).

Table 1.1 Examples of side effects associated with radiotherapy treatment with respect to the treatment site (Mohan *et al.*, 2019).

Cancer site	Side effects
Breast	Fatigue, skin irritation, breastfeeding problem, lymphedema, angiosarcoma.
Head and neck	Soreness, hair loss, oral mucositis, impaired speech function, tooth decay.
Liver	Gastritis, upper abdominal pain, gastric bleeding, nausea, and vomiting.
Thyroid	Vertigo, vocal cord paralysis, body numbness, salivary gland swelling.
Prostate	Rectal bleeding, diarrhoea, radiation cystitis, impotence, erection problems.
Lung	Breathing and swallowing difficulty, cough, breast soreness, and pneumonitis.
Ovary	Radiation cystitis, vaginal irritation, and bowel discomfort.

Despite the normal-tissue sparing advantage and the tumoricidal effectiveness of the latest-gen radiotherapy, some reports have shown that these treatments come with an expensive cost and worse patient survival than conventional treatments (Kumar *et al.*, 2021; Park *et al.*, 2021). For example, Figure 1.4 shows that the SBRT treatment alone for recurrent head and neck cancers has failed to improve the patients' overall survival compared to chemoradiation, surgery with radiation and surgery with chemoradiation. The worse outcome of SBRT is correlated to the older age of patients, patient comorbidity, advanced tumour stage, cancer history and lower biological effective SBRT dose (Park *et al.*, 2021).

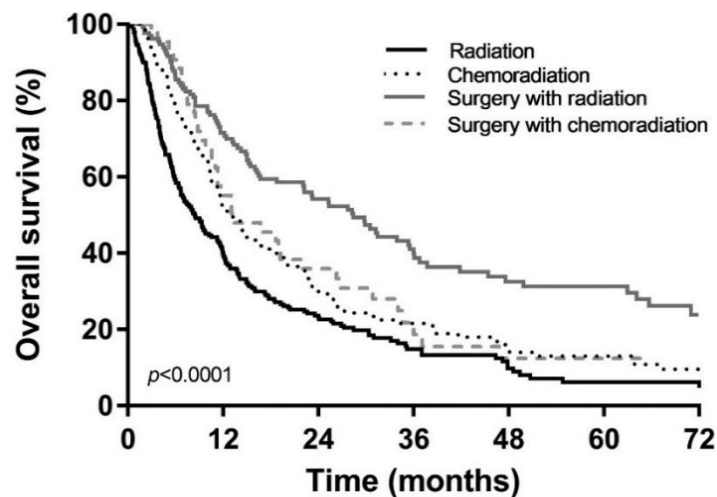


Figure 1.4 Overall survival of HNC treated with SBRT regimens with different treatment modalities (Image adapted from Park *et al.* (2021)).

Particle beam therapy also suffers from the lack of conclusive clinical evidence to support the superior theoretical efficacy of the expensive particle beam therapy over the more common photon radiotherapy techniques (Hwang *et al.*, 2020). The use of accompanying radiosensitizers may improve the efficacy significance of these advanced methods over the conventional methods.

The expensive treatment of advanced radiotherapy also makes it hardly reachable to developing countries. This is reflected by the recent statistics of global cancer incidence and mortality rate, where the mortality rate of cancer patients in Asia and Africa is higher than their incidence rate, as compared to the other region in the world (Sung *et al.*, 2021). Furthermore, due to the socioeconomic discrepancies, the distribution of radiotherapy centres worldwide is more concentrated in higher-income countries, as presented in Table 1.2. Unfortunately, the number of radiotherapy equipment per million populations significantly reduced with the country income (IAEA, 2021). Therefore, introducing contrast agents or radiosensitizers to enhance

radiotherapy efficacy is a more viable option for most global populations, especially in low-income countries.

Table 1.2 The distribution of radiotherapy centres and equipment based on the country developing index (IAEA, 2021).

Income group	Countries with RT: Countries without RT	Available RT machines	Million population	Equipment per million population
High income	62:15	8952	1245	7
Upper middle income	54:12	4102	2851	1
Lower middle income	49:14	1306	2829	0
Low income	11:19	34	643	0
Unclassified	1:4	3	1	5

Nowadays, the most recent radiotherapy technology comes with onboard imaging capabilities (Jeraj *et al.*, 2004; Gupta and Narayan, 2012; Grégoire *et al.*, 2020). The imaging procedures such as X-ray computed tomography (CT), magnetic resonance imaging (MRI) or ultrasound operated in parallel with the radiotherapy allow better localization of the tumour and real-time control of dose delivery (Grégoire *et al.*, 2020).

For example, the helical tomotherapy can use the megavoltage computed tomotherapy (MVCT) to verify the patients' positioning during the irradiation (Lee *et al.*, 2021) and result in better dose conformity to the tumour and reduced side effects to the healthy tissues (Öztunali *et al.*, 2021). However, it comes with massive shortcomings: the image quality of MVCT is poor, and the complicated setup process raise the setup uncertainty during the procedure (Lee *et al.*, 2021).

On top of that, the additional imaging radiations in parallel with the therapeutic ones will inevitably introduce additional radiation doses to the patient (Gupta and Narayan, 2012). Thus, the introduction of novel dual-modality contrast agent-radiosensitizers may help to improve the image quality and dose conformity, followed by more efficient workflow and the patients' dose management.

Figure 1.5 summarizes the concerns regarding the limitation of the latest-gen radiotherapy techniques, leading to the need for contrast and radiosensitizing agents for better tumour control. The action mechanisms of these agents can be through the reversal of radiation resistance of tumour cells, radioprotection of the surrounding healthy tissue, or by the radiosensitization of the tumour cells (Kwatra *et al.*, 2013). The agents can be fabricated in multiple forms, such as nanoparticles and functionalized molecules, with more flexibility in functionalization and personalization. This is especially important in the future, where the concept of personalized medicine is becoming more prominent (Jiang *et al.*, 2021a; Scott *et al.*, 2021). This approach may be more viable for the developing countries that already possess conventional radiotherapy equipment but cannot afford to have the latest, advanced ones. Of course, this will undeniably benefit the patients, as they will have a better chance to get improved cancer management at a considerably lower expected treatment cost.

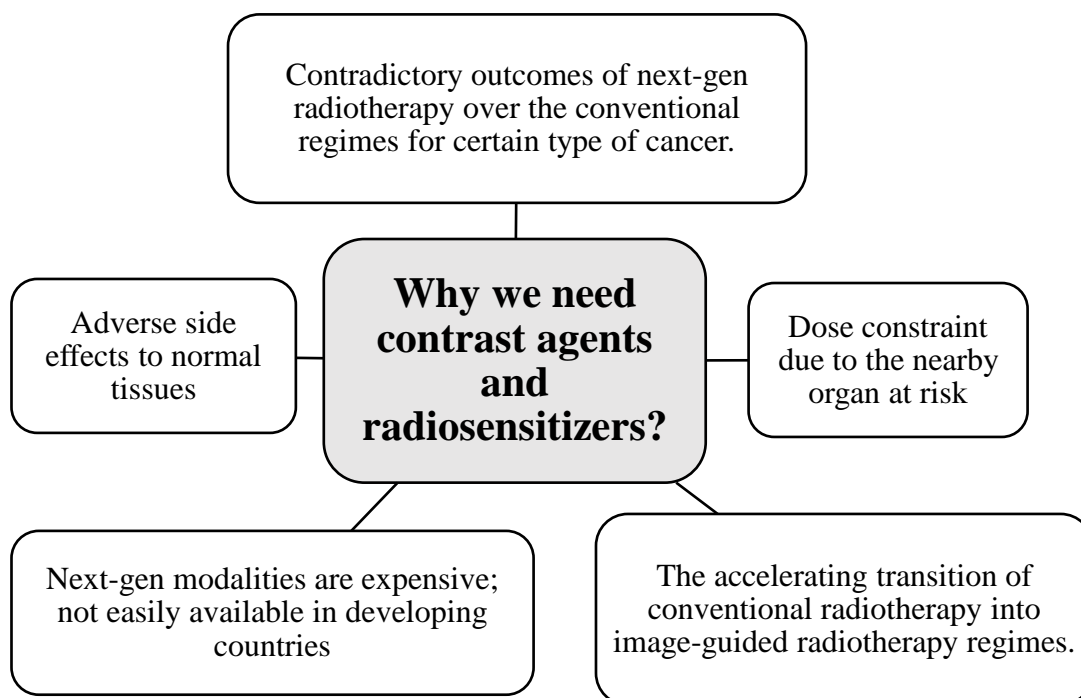


Figure 1.5 The raised concern on the need for advanced contrast agents and radiosensitizers for current cancer radiotherapy.

1.3.1 Nanomaterials as Potential Theranostic Agent

Nanoparticles are ultrafine particles between 1 and 100 nm in size (Mazari *et al.*, 2021). At this size range, the properties of a material can differ widely compared to their bulk counterpart due to the significant increment of the materials' surface area (Sun *et al.*, 2019; Yan *et al.*, 2019). Consequently, more atoms that make up the materials are readily available to interact with external media and exerts unique size-driven properties that cannot be observed within bulk materials. The nanomaterials can be observed in many forms, such as in spherical, hollow, tubular, and many more unique shapes, affecting their properties besides their size.

The nanoparticles' fabrication methods are diverse, depending on their material and the intended size and shape (Chen and Holt-Hindle, 2010; Kalaivani,

2021). Some are simpler and requires a shorter period to complete than others (Jiang *et al.*, 2021b). Most methods allow the customization of the particles' dimension just by altering one or two parameters during their fabrication process, proving the simplicity of customizing the nanoparticles depending on their purpose.

The unique properties of nanomaterials sparked much interest in their applications for many fields, including biomedical, manufacturing and energy industries (Mazari *et al.*, 2021). For example, platinum (Pt) and palladium (Pd) nanoparticles were used as electrocatalysts in fuel cell reactions (Phan *et al.*, 2021). Nanomaterials also proved to be helpful in the food and packaging industry, as they can improve the packaging's heat and flame resistance, delay the fruit ripening, and improve the shelf life of food products through their antimicrobial properties (Tiwari *et al.*, 2021).

The medical fields are not left behind in venturing the possible applications of nanomaterials to improve healthcare. The combination of the field of medicine and nanotechnology for disease prevention and treatment gave birth to the area of nanomedicine (Liu *et al.*, 2020b; Bernal *et al.*, 2021). The global market of nanomedicine is flourishing every year. Many nanoparticle-based pharmaceutical products are already approved by Food and Drug Administration (FDA) and currently circulating in the market (Gadekar *et al.*, 2021). It was projected that this industry's compound annual growth rate would show a 14 % increase from 2017 until 2022 (Evers, 2015).

The significant annual growth of the nanomedicine industry was fertilized by the favourable characteristics of nanoparticles for biomedical applications. For example, the nanoparticles' surface was found to be easily modified, labelled, or

tagged with other biocompatible compounds (Prasad *et al.*, 2020). These processes, collectively termed as surface functionalization, offers flexibility in developing a nanomaterial-based non-toxic drug. Nanoparticles also can be functionalized with the compounds that are primarily taken up by a specific organ, allowing them to specifically accumulate in the intended organ (Khot *et al.*, 2021). Nanoparticles are also candidates as excellent agents in the targeted drug therapy or diagnostic procedures in the oncology field (Sun *et al.*, 2019; Liu *et al.*, 2020b; Khot *et al.*, 2021). The underdeveloped blood vessels within the tumour due to angiogenesis allows the particles smaller than 100 nm to pass through their endothelial cell layers unhindered, causing significant accumulation of the nanoparticles within the tumour mass. The ease of functionalization of the nanoparticles' surface extends their potential to be a more efficient, safe, and accurate therapeutic agent.

With the unending array of nanoparticles' potentials, one needs to find the correct combination of material, size, shape, and surface properties to make up a promising nanoparticle in their intended field. In this work, the Platinum Nanodendrite's (PtND) primary intended application is to be an excellent theranostic agent, an agent that can be used as a contrast agent in diagnostic radiology and a radiosensitizer in radiation therapy. With the advancement of image-guided radiotherapy, the development of accompanying theranostic agents is crucial as insurance to give the best curative or palliative treatment the patients can get out of the already expensive cancer treatment regimes.

1.4 Problem Statement

Radiotherapy has been used extensively to treat cancer aside from surgery and chemotherapy. The procedure boasts the advantage over surgery or chemotherapy because of its minimally or non-invasive procedure. Radiotherapy patients also usually do not need to be warded to get the treatment, and the procedure only requires a short amount of time per session.

Albeit all those benefits, radiotherapy is not without downsides. Without surgery, the tumour localisation within the patient's body mainly relies on radiographic imaging during radiotherapy simulation. Some tumours can be easily distinguished from the surrounding bodily materials, but some are not. Careful delineation of the treatment area needs to be performed by the oncologist before the actual treatment to avoid any mistakes during the irradiation, especially when the targeted tumour is located nearby radio-sensitive organs.

The radiations are also projected from outside the patients' body toward the target area within the body; thus, the tissues located between the skin and that target also received a portion of the radiation dose. With the advancement of radiotherapy modality, treatments nowadays can be performed in conjunction with real-time imaging. Thus, there is a need to develop theranostic agents that can cooperatively improve the contrast of the tumour in the images for accurate tumour localization and amplify the dose to the targeted tumour, which can also spare the healthy tissues from unnecessary radiation doses.

Nanoparticles have been studied extensively in the past decade to be used as theranostic agents due to their unique pharmacokinetics and the simplicity in their fabrication and functionalization methods. Until now, only a few nanoparticle

theranostic agents have been developed using high-Z materials to harvest their high interaction cross-section properties, such as gold and hafnium nanoparticles. However, the results are still inconclusive, and the researchers are yet to achieve a consensus on which nanoparticles' material and morphology combination are the best to create the optimal theranostic agent. Relevant literature has reported the theranostic capabilities of gold and hafnium nanoparticles, yet no studies have specifically evaluated the theranostic potential of platinum NPs.

Few studies have characterized the interaction between radiation and platinum-based NPs, yet their tested parameters are limited. To our knowledge, none of them has addressed the contrast enhancement effect of platinum nanodendrites (PtNDs) in diagnostic radiology, let alone the correlation between the contrast enhancement with the PtND size. The same goes for the radiosensitization effect of platinum NPs in clinical radiotherapy. Their tested parameters in most studies are mostly restricted to a single type of radiotherapy or size of nanoparticles.

Furthermore, while many studies have evidenced the contrast enhancement and radiosensitization effect of high-Z nanoparticles, the understanding of the mechanisms behind their effect is still inadequate. This is especially true with platinum NPs. Platinum NPs are well-known as radical scavengers, yet they still evidenced a significant radiosensitization effect in several radiotherapy types. This creates a paradox in elucidating the mechanism behind the radiosensitization by platinum NPs, as it is also widely accepted that radicals such as reactive oxygen species (ROS) play a significant role in inducing radiation damage toward the biological medium.

Therefore, this work is performed to evaluate the theranostic potential of PtNDs, as well as elucidating the factors and mechanisms that may affect their performance as an agent in both diagnostic radiology and radiotherapy.

1.5 Objective of Study

The general objective of this study was to evaluate the potential of Platinum Nanodendrites (PtNDs) as a novel theranostic agent; an agent that can act as both contrast agent in diagnostic radiology, and as radiosensitizer in radiotherapy. This general objective encompassed the following specific objectives: -

- i. To characterize the PtNDs with an optimal condition for radiosensitizer and contrast agent application.
- ii. To investigate the biocompatibility of various sizes of PtNDs.
- iii. To assess the contrast enhancement of PtNDs in diagnostic imaging.
- iv. To evaluate the radiosensitization effect of PtNDs under the irradiation of different types of radiotherapy beams.
- v. To verify the feasibility of PtNDs as a theranostic agent.

1.6 Scope of Study

In this work, the PtNDs were synthesized using the chemical reduction method reported by Ridhuan *et al.* (2014). This study's primary aim was to characterize the potential of PtNDs as a theranostic agent. Therefore, the characterizations of the fabricated PtNDs were done to elucidate the factors that may affect the theranostic capabilities of PtNDs, such as the PtNDs' morphology, pH, elemental constituents, and their biocompatibility. The contrast enhancement studies were performed on

phantoms and compared with the commercial iodinated contrast agent. On the other hand, the radiosensitization effects of PtNDs were assessed through the *in-vitro* method. Only three radiotherapy types were used in this work, namely photon, electron, and proton beam radiotherapy. However, we did not evaluate the energy-dependent and cell-dependent radiosensitization effect due to time constraints and resource limitations. These parameters are suggested in the future recommendations at the end of this thesis.

1.7 Thesis Outline

This thesis is divided into six (6) chapters, starting from the Introduction, Literature Review, Methodology, Result, Discussion, and Conclusion, respectively. Chapter 1 starts with the current global cancer prevalence and the latest technological advancements in cancer management, especially in radiotherapy. Fundamentals of radiobiology are introduced in this chapter to understand the basic mechanisms behind the cell-killing effect of radiotherapy treatment. It is followed by insight into the several limitations in the current-generation radiotherapy regimes, which lead to the suggested importance of contrast and radiosensitizing agents to be implemented in parallel with the systems. Next, we briefly reviewed the current progress of research on nanoparticle-based theranostic agents and the unique characteristics of nanomaterials that fuel the interest. The introduction section is capped with the problem statement and the research objective of this work, which become the backbone of this thesis.

Chapter 2 contains the review of relevant literature, starting with platinum nanoparticle synthesis and characterization methods. Next, current progress in the

application of high-Z nanoparticles as theranostic agents, specifically in the field of radiation oncology, is discussed. The mechanisms behind the radiosensitization effect of these agents are discussed in detail, which is separated into three distinct categories, namely physical, chemical, and biological mechanisms.

Chapter 3 comprises a detailed explanation of the experimental procedures performed in this work, starting with the Platinum Nanodendrites (PtNDs) synthesis and characterization, their biocompatibility assessment, the contrast enhancement studies, and the radiosensitivity evaluation of the fabricated PtNDs. The chapter is capped with the statistical analysis used throughout the work.

Chapter 4 contain the results of this research. The results are compared with findings from previous literature in Chapter 5. The findings are reviewed regarding their similarity and differences and the suggested mechanism that led to their respective conclusions. The influence of PtNDs size on their biocompatibility, contrast enhancement and radiosensitization effect is then justified with the support of current knowledge in the field.

Finally, all these results are summarised and concluded in Chapter 6. The limitations of this research and the relevant recommendations for future studies are also written in this chapter. The supporting data and information that may aid the presentation of this thesis can be found in the Appendices.

CHAPTER 2

LITERATURE REVIEW

This chapter is comprised of three main topics. The first topic is about producing platinum nanoparticles for many application types and the various common ways of characterizing the fabricated particles before their application. The next part revolved around the current research and applications of high-Z nanoparticles as theranostic agents. Finally, this chapter rounds up the radiosensitization effect of high-Z nanoparticles and the mechanisms behind the effects (physical, chemical, biological mechanisms), which enticed the researchers to delve into the applications of these materials as radiotherapy sensitizing agents.

2.1 The Fabrication and Characterization of Platinum Nanoparticles

2.1.1 Multiple Pathways of Nano-platinum Production

Platinum nanoparticles (PtNPs) can be fabricated through many different methods. Chen and Holt-Hindle (2010) have summarized the methods to synthesize the PtNPs into five categories: - hydrothermal and solvothermal techniques, sol-gel methods, electrochemical deposition, physical synthesis techniques and electroless deposition.

On the other hand, Stepanov *et al.* (2014) also introduced few categories to classify the PtNP synthesis methods. The categories were divided into two major types. The first group involves chemical solutions in the fabrication process, and the latter integrates physical techniques. Chemical preparation includes shape-controlled synthesis method, chemical reduction method, and curing one-step process in polymer,

while physical techniques comprise co-sputtering and electron beam evaporation method, ion implantation method, surface etching-combined ion implantation, and laser ablation in solution. To sum up, we summarized the methods for PtNP fabrication into seven major types presented in Figure 2.1.

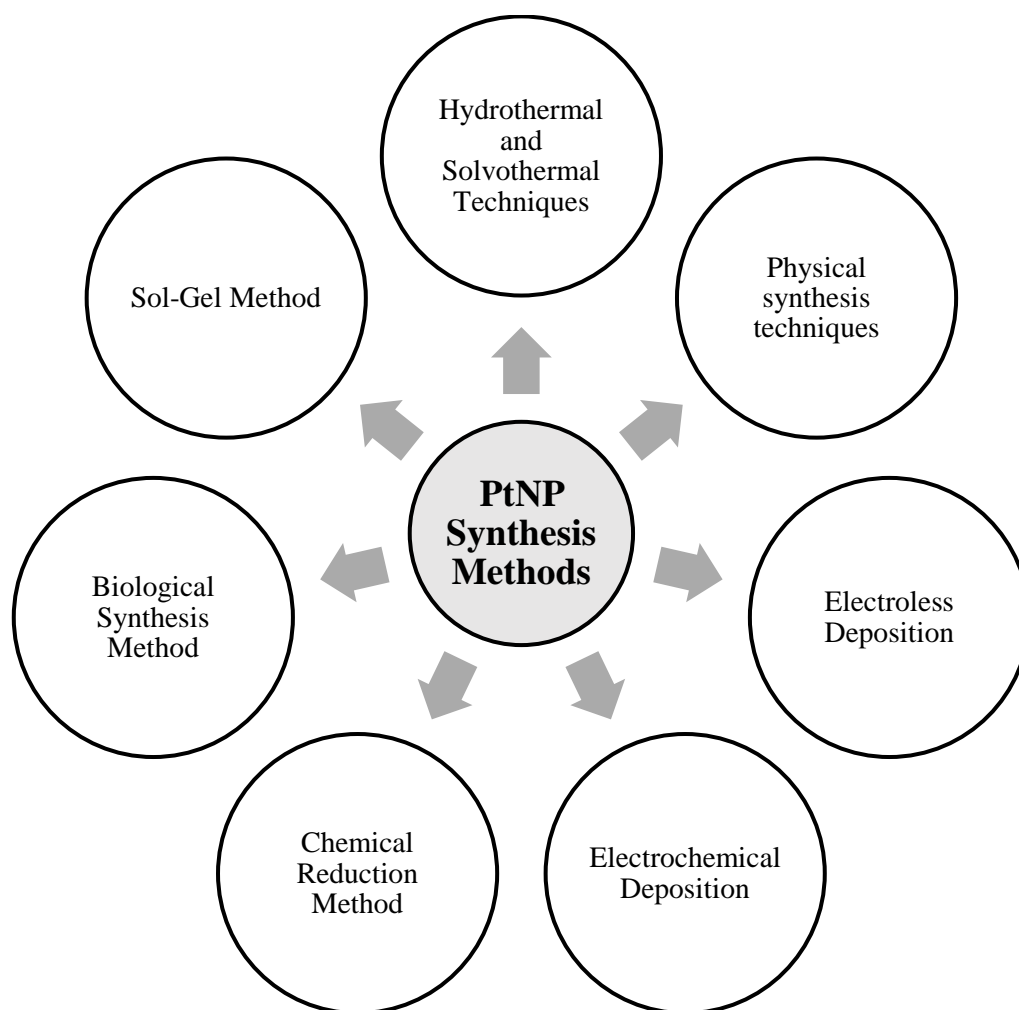


Figure 2.1 Categories of platinum nanoparticle synthesis methods.

The hydrothermal and solvothermal method allows an easy process to produce Pt, Pt-based binary, and Pt-based ternary nanomaterials of distinct shapes and sizes. Hydrothermal involve a heterogeneous reaction, which takes place in aqueous solvents

under high temperature and pressure condition while solvothermal processes differ in the use of nonaqueous solvents. This technique usually takes place in closed systems, such as Teflon lined autoclaves enclosed in steel vessels. Hydrothermal and solvothermal methods require inexpensive equipment and can be completed within a day. However, the need to operate in high temperatures and pressure hinders the possibility to observe the growth of the synthesized nanomaterials.

The sol-gel method is a wet-chemical technique that efficiently produces Pt and Pt-based nanostructures of small dimensions with uniform size and distribution. Platinum nanoparticles can be fabricated on many supporting materials such as silicate, aluminium, titanium, and carbon using this method, which is useful in developing highly efficient Pt-based catalysts for fuel cells and other applications.

Physical syntheses are the processes whereby the precursor material undergoes no physical changes. There are many different methods under physical synthesis techniques, such as sputtering technique, ion or electron beam deposition, laser ablation, and various irradiation types. The fabrication conditions, the concentration of reagents, and the presence of stabilizers in these physical synthesis methods can be tuned to control the product composition, morphology, and properties. In addition, physical synthesis methods permit the production of nanoparticles without impurities and free of surfactant, allowing direct access of the reactants to the surface-active sites of metal nanoparticles.

The electrochemical deposition method involves using a two- or three-electrode electrochemical system, with the electrolyte serving as the source of Pt and conducting medium. Deposition occurs by controlling either the electrode potential or the current density of the electrochemical cell. This method is used to fabricate thin